

# PROCEEDINGS OF SPIE

[SPIDigitalLibrary.org/conference-proceedings-of-spie](https://spiedigitallibrary.org/conference-proceedings-of-spie)

## Design of a multistep phase mask for high-energy THz pulse generation in ZnTe crystal

Yuri H. Avetisyan  
Armen Makaryan  
Vahe Tadevosyan

**SPIE.**

# Design of a multistep phase mask for high-energy THz pulse generation in ZnTe crystal

Yuri H. Avetisyan\*, Armen Makaryan, Vahe Tadevosyan

Dept. of Microwave Eng., Yerevan State University, 1 Alex Manoogian Str. Yerevan, 0025 Armenia

## ABSTRACT

A new scheme for generating high-energy terahertz (THz) pulses by optical rectification of tilted pulse front (TPF) femtosecond laser pulses in ZnTe crystal is proposed and analyzed. The TPF laser pulses are originated due to propagation through a multistep phase mask (MSPM) attached to the entrance surface of the nonlinear crystal. Similar to the case of contacting optical grating the necessity of the imaging optics is avoided. In addition, introduction of large amounts of angular dispersion is also eliminated. The operation principle is based on the fact that the MSPM splits a single input beam into many smaller time-delayed “beamlets”, which together form a discretely TPF in the nonlinear crystal. The dimensions of the mask’s steps required for high-energy THz-pulse generation in ZnTe and widely used lithium niobate (LN) crystals are calculated. The optimal number of steps is estimated taking into account individual beamlet’s spatial broadening and problems related to the mask fabrication. The THz field in no pump depletion approximation is analytically calculated using radiating antenna model. The analysis shows that application of ZnTe crystal allows obtaining higher THz-pulse energy than that of LN crystal, especially when long-wavelength pump sources are used. The proposed method is a promising way to develop high-energy, monolithic, and alignment-free THz-pulse source.

**Keywords:** Terahertz, THz generation, optical rectification, multistep phase mask.

## 1. INTRODUCTION

Over the last 20 years, dramatic improvements have been made in the generation of intense THz pulses, which are of interest for various research fields such as nonlinear spectroscopy [1, 2], material science [3, 4] and development of a new compact charged particle and x-ray sources [5, 6]. Among various methods of THz pulse generation, the optical rectification (OR) in a nonlinear optical (NLO) crystal is one of the most commonly used techniques because of its simplicity and basic requirements for table-top sized generator. In addition, it has emerged as the most powerful way to generate high energy THz pulses, and by using a novel organic crystal DSTMS it resulted in the highest THz pulse energy (0.9 mJ) generated to date [7]. The spectrum obtained from organic materials is typically centered in the 2 to 10 THz range, whereas THz sources with lower frequencies are needed for many applications, in particular for particle acceleration [6, 8].

The lithium niobate (LN) crystal is also an excellent material for THz generation, especially due to its high second order nonlinear coefficient. Usually, the THz spectrum radiated by LN crystal is concentrated in the low frequency region  $\nu < 1.5$  THz. The main drawback is its inability of the collinear phase-matched THz generation due to the large difference between the THz refractive index  $n_{THz}$  and the optical group index,  $n_g$ . Generally, the phase-matched THz generation is automatically obtained in the direction determined by Cherenkov radiation angle  $\theta_{Ch} = \cos^{-1}(n_g/n_{THz})$ , when LN crystal is illuminated by a very narrow (as compared to the THz wavelength in the material) aperture beam. However, for powerful THz generation, wide aperture optical beams are required to escape intensity dependent effects in nonlinear crystal such as multiphoton absorption at pump wavelength and cascading processes together with a strong angular dispersion [9]. For this reason, special efforts have been undertaken to compensate the phase mismatching in the beam cross-section plane. Application of a binary phase mask in front of the LN crystal provides quasi-phase matched (QPM) THz generation, but only in a narrow spectral bandwidth [10]. It results in increase of the THz-pulse energy, but not in increase of the THz peak power.

The exclusive solution for broadband THz-pulse generation in LN crystal is application of the tilted-pulse-front pumping (TPFP) technique [11]. In a conventional setup the pump beam is reflected off a grating to acquire a tilted-pulse-front

(TPF), which is then subsequently imaged onto the crystal using a lens or a telescope. Using this method, THz pulses with energy as high as 0.4 mJ [12] and pump-to-THz conversion efficiency  $\eta = 3.8\%$  [13] were obtained, using femtosecond pulses at 1030 nm central wavelength. However, further increase in THz generation performance is challenging because of serious limitations [9, 12-14]. Significant problems inherent to the common TPF scheme are the imaging errors in NLO crystal and the temporal broadening of the pump pulse due to the angular dispersion. Using a stair-step echelon (instead of a reflecting grating) allows obtaining discretely TPF laser pulses without degradation of the pulse duration. The generation of THz-pulses with high conversion efficiency  $\eta$  close to record 0.35% (at pump wavelength of 800 nm [14]) and energy of 3.1  $\mu\text{J}$  has been reported using 70 fs laser pulses at 800 nm central wavelength [15]. However, the obtained THz-pulse energy is significantly smaller than it was reported by using common TPF scheme at the same pump wavelength [14, 16]. Probably it is related to imperfections in the stair-step echelon fabrication and non-optimal duration of the pump pulses. Recently, it was theoretically shown that the conversion efficiency up to 5% can be obtained using 0.5 ps pump pulses [17].

To avoid problems related to the imaging errors in NLO crystal, a contact grating (CG) method has been proposed, in which a transmission grating is placed at the crystal's entrance surface [18]. Addition advantage of the CG scheme is the opportunity to use a parallel-plate form NLO crystal that eliminates the spatial non-uniformity of the interaction length. It results in a good quality THz beam and extremely high THz field in the focus of the THz-optics. Recently, this method has been realized using a thin-film contact grating deposited on LN [19] and contact grating etched on ZnTe crystals [20]. In the experiment with LN crystal the Yb:YAG laser pulses of 1.3 ps duration at 1030 nm wavelength were used. The generated THz pulse energy showed a quadratic dependence on the pump laser energy, which indicates that complex phenomena such as cascade processes and multiphoton absorption (MPA) did not occur. However, the THz pulse energy was only 0.22  $\mu\text{J}$  at pump laser energy of 3.5 mJ, corresponding to a conversion efficiency of  $6.3 \times 10^{-5}$ . Intense THz-pulses with energy of 2.3  $\mu\text{J}$  and high conversion efficiency  $\sim 0.3\%$  were generated in the experiment with ZnTe crystal thanks to pumping at an infrared wavelength sufficiently long to suppress both two- and three-photon absorptions. Besides, fabrication of CG for ZnTe crystal is relatively easy as required TPF angle is below  $30^\circ$ , in contrast to LN crystal, where it is about  $63^\circ$ . It should be noted that in CG scheme the problems related to temporal broadening of the pump pulse are not eliminated, which can still lead to reduction of the generated THz-pulse bandwidth and energy.

In this paper, we present a new scheme of THz-pulses generation by OR in NLO crystal using multistep phase mask (MSPM) to provide discretely TPF laser pulses in the crystal. It was previously proposed and analyzed [21], but obtained results are not physically transparent, moreover, only LN crystal was considered. Here we extend the analysis and show that application of ZnTe crystal is more preferable, especially when a longer wavelength pump source is applied. The operation principle of the MSPM is similar to that of the stair-step echelon [15], however, MSPM works in the transmittance regime, which is beneficial for avoiding the imaging errors in the NLO crystal. In contrast to the CG method, introduction of large amount of angular dispersion in the proposed scheme is eliminated as well.

## 2. MULTISTEP PHASE MASK DESIGN

The THz generation in nonlinear crystal with attached MSPM is schematically presented in Fig. 1. The optical beam propagation through the MSPM results in the formation of an ensemble of spatiotemporal shaped femtosecond pulses.

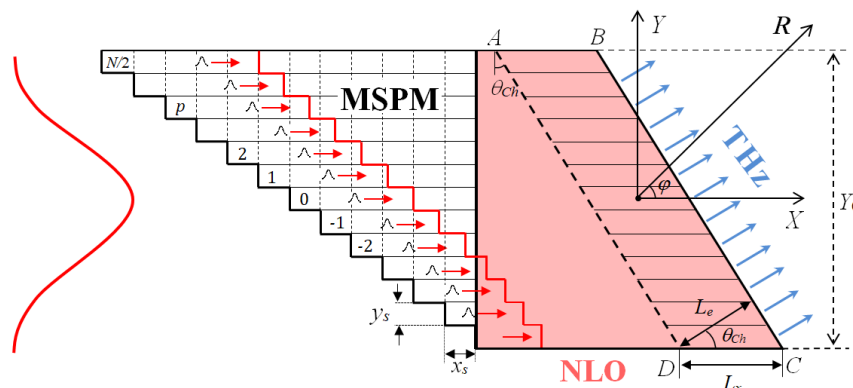


Fig. 1. Schematic view of THz generation in nonlinear optical (NLO) crystal with attached multi-step phase mask (MSPM).

As it is seen from Fig. 1, MSPM splits a single input beam into  $(2N + 1)$  time-delayed “beamlets”, which are propagating through every  $p$ -step of the mask with a time delay  $\tau_p = p\tau$ , where  $\tau = x_s(n_{gm} - 1)/c$  is the temporal shift of pulses in the neighboring steps,  $n_{gm}$  is the group index of the mask medium,  $x_s$  is the step length and  $c$  is the speed of light,  $p = 0, \pm 1, \pm 2 \dots N/2$  is an integer number. In the crystal every  $p$ -beamlet radiates a THz-pulse in the form of Cherenkov wedge propagating at an angle  $\theta_{Ch} = \cos^{-1}(n_g/n_{THz})$ , where  $n_{THz}$  is the THz refractive index at  $\omega_{THz}$  frequency and  $n_g$  is the optical group index. For constructive interference of these THz pulses, certain relationship between temporal delay  $\tau$  and beamlets distance  $y_s$  has to be satisfied. To establish that relationship we assume that the pump beam has one of the transverse dimensions much larger than the other, which allows using a simple 2-dimensional (2-D) theoretical model.

The analysis of THz generation in the mask covered NLO crystal [22] showed that the phase-matched THz emission at Cherenkov angle takes place, if the mask provides linearly varying delay time  $\tau = y(n_{THz}\sin\theta_{Ch}/c)$ . By approximating this dependence via a staircase function we conclude that the steps thickness of MSPM and the delay time of the laser pulses have to satisfy the following Eq. (1)

$$y_s = \frac{c}{\sqrt{n_{THz}^2 - n_g^2}} \tau. \quad (1)$$

Obviously, for high-accuracy approximation small  $y_s$  is desirable. However, to cover a certain size of the NLO crystal, large steps number  $N_s$  is required, complicating the MSPM fabrication. The Cherenkov-type THz emission from a separate  $p$ -beamlet is not phase matched in the direction perpendicular to the beamlet’s propagation. Using radiating antenna model [23] it has been shown that phase mismatching along the  $Y$ -axis results in reduction of the generated field by a factor  $F = \text{sinc}(\pi y_s/2l_c)$ , where  $l_c = \lambda/2n_{THz}\sin\theta_{Ch}$  is the coherence length and  $\lambda = 2\pi c/\omega$  is the wavelength. In essence, the factor  $F$  indicates THz field decrease caused by discretely TFPF instead of a common continuous one.

Nowadays the NLO crystals with discretely modulated nonlinear coefficient are widely used as laser radiation frequency converters [24, 25]. Due to the quasi-phase-matched (QPM) nonlinear interaction the generated field is reduced by  $\pi/2$  times in comparison with the perfectly phase-matched case. Using the same value for the  $F$  factor we determine the steps thickness of the MSPM for the condition  $y_s = y_0 \equiv l_{cTHz}$ , where  $l_{cTHz}$  is the coherence length  $l_c$  at the designed (central) wavelength of THz spectrum,  $\lambda_{THz}$ . Thus, the MSPM step thickness  $y_0$  is given by

$$y_0 = \frac{\lambda_{THz}}{2\sqrt{n_{THz}^2 - n_g^2}}. \quad (2)$$

It is instructive to note that the same Eq. (2) determines the spatial period of the 1-D binary mask used for QPM generation of multi-cycle THz radiation [10, 26]. The multi-cycle THz radiation was formed due to repetition of the single-cycle THz pulses (radiated by each  $p$ -beamlet), which reached to exit surface of LN crystal with delay  $\tau_p = pT_{thz}/2$ , where  $T_{thz} = \lambda_{THz}/c$  is the period. In our case, the 2-D MSPM introduces the same negative temporal shift between the radiated single-cycle THz pulses resulting in its constructive temporal overlapping. From above it follows that temporal delay between laser pulses propagating in the neighboring channels has to be  $\tau = T_{thz}/2$ . Using  $\tau = x_s(n_{gm} - 1)/c$ , we obtain the necessary step length  $x_0$  given by

$$x_0 = \frac{\lambda_{THz}}{2(n_{gm} - 1)}. \quad (3)$$

Thus, Eqs. (2) and (3) allow calculating both the thickness and the length of the MSPM step. From these equations one can easily verify that in the crystal the MSPM provides discretely TFPF at an angle  $\gamma$  equal to the Cherenkov angle  $\theta_{Ch}$ . Indeed, the spatial shift of the laser pulse-fronts in the neighboring beamlets is  $c\tau/n_g$  and therefore the tilt angle in crystal is given by

$$\tan \gamma = \frac{c\tau}{y_0 n_g}. \quad (4)$$

By substituting  $\tau = T_{thz}/2$  and using Eq. (2) for  $y_0$ , one obtains that  $\gamma = \theta_{Ch}$ .

### 3. RESULTS AND DISCUSSIONS

#### 3.1 MSPM structures for using with LN and ZnTe crystals

Let us now estimate the step sizes of MSPMs intended for using with LN and ZnTe crystals. For both cases the central wavelength of the THz spectrum is chosen to be  $\lambda_{THz} = 300 \mu\text{m}$ . The pump wavelengths are chosen respectively to be  $\lambda_p = 1.7 \mu\text{m}$  for ZnTe and  $\lambda_p = 1.03 \mu\text{m}$  for LN crystals to suppress three-photon absorption in the crystal and associated free-carrier absorption in the THz range [8, 12, 19, 20]. As the materials for MSPM preparation the semiconductors GaAs or GaP are attractive. They have a large group index  $n_{gm}$  that is favorable for obtaining necessary temporal delay in the mask at the shorter distances. Moreover, the techniques of stacking GaP or GaAs thin parallel-plates are well developed [27-29]. It gives opportunity for MSPM preparation by bonding set of GaP or GaAs plates having different lengths along  $X$ - or  $Y$ - axes. In Fig. 1, the interfaces inside the MSPM are shown by horizontal (solid) lines in the former case and vertical (dotted) lines in the latter case. However, MPA can be strong in these materials, especially when wavelength of the pump laser is not sufficiently longer. For this reason the wide band-gap materials such as Sapphire and GaN are more preferable. In the following, assuming the use of synthetic Sapphire, we set the group index to be  $n_{gm} = 1.75$ . The mask fabrication can be implemented by bonding technique or by etching stairs on the entrance surface.

According to Eq. (3) for chosen  $\lambda_{THz}$  and  $n_{gm}$  the step length of the MSPM is  $x_0 = 200 \mu\text{m}$ , independent of the NLO crystal material. From Eq. (4) it follows that the required steps thicknesses of MSPM are  $y_0 = 33.7 \mu\text{m}$  and  $y_0 = 98 \mu\text{m}$  for 1.3% Mg-doped stoichiometric LN (sLN) crystal ( $n_g = 2.2$  [30],  $n_{THz} = 4.96$  [31]) and ZnTe crystal ( $n_g = 2.79$  [32],  $n_{THz} = 3.18$  [33]), respectively. Obviously, fabricating an MSPM for ZnTe crystal is easier due to larger step dimension  $y_0$ . In addition, larger  $y_0$  is favorable for minimizing the laser beam diffraction.

The Rayleigh ranges of the beamlets are  $R \approx 31 \text{ mm}$  (6 mm) in the masks designed for ZnTe (sLN) crystals, respectively. The path length of  $p = 0$  beamlet propagating in the central part of the MSPM is  $L = Nx_0/2$ , where  $N$  is the number of steps in the mask. In order to neglect the effect of the beamlets broadening, we consider  $L \leq R/2$  that corresponds to the maximal number of the steps  $N_1 = 155$  and  $N_2 = 30$  for ZnTe and sLN crystals, respectively. Certainly, in the former case the number of steps is too big for MSPM fabrication, especially if thin plates bonding technique is used. In following, in order to maintain equal conditions for the both crystals, it is assumed that  $N_1 = N_2 = 30$ . Also we take into account that a stack of thirty 106  $\mu\text{m}$ -thick plates has been recently fabricated by room-temperature bonding technique [29]. Using  $N = 30$  and above calculated  $y_0$ , the maximal mask's sizes along the  $Y$ -axis are estimated to be  $Y_0 = 3 \text{ mm}$  (1 mm) for ZnTe (sLN) crystals, respectively. The larger beam size is beneficial for higher pump power application to the crystal. This, together with a smaller THz absorption, can lead to higher THz power generation in ZnTe crystal compared with LN crystal.

The comparative analysis of THz-pulse generation in ZnTe and LN crystals has been done in many publications [34, 35]. Some advantages of ZnTe crystal related to easier MSPM fabrication and enabling application of a large aperture pump beam were already mentioned. However, LN crystal has about 2.5 times higher second order nonlinear coefficient  $d_{eff}$ . In addition, in the case of ZnTe crystal the dependence of THz-pulse energy on the pump intensity  $I_{av}$  deviates from quadratic relation above the average intensity  $I_{av} \approx 13.5 \text{ GW/cm}^2$  [8, 20], whereas for LN crystal such dependence holds up to  $I_{av} \approx 20 \text{ GW/cm}^2$  [17, 35].

#### 3.2 THz-pulses energies in LN and ZnTe crystals

Here we estimate the THz pulse energy spectral density  $e_{THz}(\omega)$  using radiating antenna model [23, 36] with some simplifying assumptions. We suppose that only a crystal's portion restricted by the area  $ABCD$  is effectively involved in THz generation (Fig.1) and crystal is surrounded by linear medium having the same THz refractive index. The effective interaction length  $L_e = 2/\alpha$  is determined by the inverse value of THz-wave absorption  $\alpha$  at the designed central frequency of THz spectrum  $\omega_{THz} = 2\pi c/\lambda_{THz} = 2\pi \text{ THz}$ . The intensity of the pump pulses is chosen to be lower than the values at which the cascade nonlinear processes and multiphoton absorption become noticeable. It is also assumed that the pump pulse has Gaussian temporal and spatial profiles, which do not change during propagation in the crystal. Thus, the electrical field of the individual  $p$ -beamlet is given by

$$E_p(x, y, z, t) = E_0 G(z, y) \exp \left[ -\frac{(t - p\tau - xn_g c^{-1})^2}{2\tau_L^2} \right] \cos(\omega_0 t - k_0 x), \quad (5)$$

where  $p = 0, \pm 1, \pm 2 \dots N/2$ ,  $\tau = x_0(n_{gm} - 1)/c$  is the delay provided by the each step,  $G(z, y) = \exp[-(z/r_z)^2] \cdot \exp[-(y/r_y)^2]$  is the Gaussian beam shape factor,  $r_y$  and  $r_z$  are the beam waist radii,  $k_0 = \omega_0 n_0/c$  is the wavenumber at frequency of the laser radiation  $\omega_0$ ,  $\tau_L$  is the pulse duration related to the standard full width at half maximum (FWHM) by  $\tau_{FWHM} = 2(\ln 2)^{1/2} \tau_L = 1.66 \tau_L$ , and  $E_0$  is the amplitude given by

$$E_0 = \sqrt{\frac{4e_L W}{\pi^{3/2} n_0 r_y r_z \tau_L}}, \quad (6)$$

where  $e_L$  is the energy of the pump pulse in the crystal and  $W = (\mu_0/\epsilon_0)^{1/2}$  is the free space impedance.

The spectral distribution of the nonlinear polarization driven by  $p$ -beamlet is determined by Fourier transform of the pump pulse intensity [37] and it is given by

$$P_p(x, y, z, \omega) = \frac{2\sqrt{\pi} \tau_L \epsilon_0 d_{eff} W I_0 e^{-2y^2/r_y^2} e^{-2z^2/r_z^2}}{n_0} \exp\left[-\left(\frac{\omega^2 \tau_L^2}{4}\right) - i\omega\left(p\tau + \frac{n_g}{c} x\right)\right], \quad (7)$$

where  $I_0 = n_0 E_0^2/2W$  is the peak beam intensity, which is related to the average intensity by  $I_{av} \approx 0.53 I_0$ . It is instructive to note that the average intensity  $I_{av} = \epsilon_L/\tau_{FWHM} \pi r_y r_z$  is mostly used in experimental estimation of the laser beam intensity.

The THz field produced by  $P_p$  is calculated by considering nonlinear medium as radiating antenna fed by a current  $j_z(x, y, z, \omega) = i\omega P_p(x, y, z, \omega)$  [23]. By such way the THz field driven by  $p$ -beamlet in the far-field approximation is given by

$$E_{\theta_p}(\vec{R}, \omega) = \frac{\mu_0 \omega^2 e^{-ikR} \sin \theta_z}{4\pi R} \int_{p y_0 - y_0/2}^{p y_0 + y_0/2} dy \int_{-y \tan \theta_{ch} - L_x/2}^{-y \tan \theta_{ch} + L_x/2} dx \int_0^{Z_0} P_p^{NL}(\omega, x, y, z) \exp\left[i(k_z z + k_x x + k_y y)\right] dz, \quad (8)$$

where  $Z_0$  is the NLO crystal dimension along the  $Z$ -axis,  $L_x = L_e/\cos \theta_{ch}$  is the effective length along the  $X$ -axis,  $\vec{R} = (R, \theta_z, \varphi)$  is the position vector of the point of field observation,  $k_z = k \cos \theta_z$ ,  $k_x = k \sin \theta_z \cos \varphi$  and  $k_y = k \sin \theta_z \sin \varphi$  are the respective projections of the THz wave-vector  $\vec{k} = k(\vec{R}/R)$ ,  $k = \omega n_T(\omega)/c$  is the THz wavenumber, and  $n_T(\omega)$  is the frequency dependent THz refractive index.

First, the integration over variable  $z$  is performed, since dependence of the nonlinear polarization on  $z$ -coordinate is determined only by Gaussian shape factor  $G(z, 0) = \exp[-2(z/r_z)^2]$ . By considering that the laser beam is completely inside the crystal  $r_z \ll Z_0/2$ , the integration limits can be replaced by  $\pm \infty$ . As a result of the integration we obtain the factor  $H(\omega, \theta_z)$  given by

$$H(\omega, \theta_z) = \sqrt{\frac{\pi}{2}} r_z \exp\left[-\left(\frac{r_z \omega n_T \cos \theta_z}{2\sqrt{2}c}\right)^2\right] \quad (9)$$

The above equation indicates that the THz radiation pattern lies mainly in the azimuthal plane ( $\theta_z = \pi/2$ ). The angular width of the radiation maximum at  $1/e^2$  level is determined by

$$\Delta \theta_z = \frac{2\sqrt{2} \lambda_{THz}}{\pi n_{THz} r_z} \quad (10)$$

Next, the integration of Eq. (8) over  $x$  and  $y$  is performed using  $\theta_z = \pi/2$  and assuming Gaussian beam shape factor  $G(0, y) \approx \exp[-2(py_0/r_y)^2]$ , i.e. it does not depend on  $y$  within the integration limits because  $r_y \gg y_0$ . As a result, we obtain that in the frequency domain the THz field radiated by  $p$ -beamlet is given by

$$E_{zp}(\omega, \varphi) = \frac{Ae^{-ikR}}{R} I_0 D(\omega, \varphi) F(\omega, \varphi) \exp \left[ -2 \left( \frac{py_0}{r_y} \right)^2 - \left( \frac{\omega\tau_L}{2} \right)^2 + ip(K(\omega, \varphi)y_0 - \omega\tau) \right], \quad (11)$$

where  $A = \frac{\omega^2 d_{eff} W L_x y_0 r_z \tau_L}{2\sqrt{2}c^2 n_0}$ ,  $F(\omega, \varphi) = \text{sinc}\left(\frac{\Delta k L_x}{2}\right)$ ,  $\Delta k = k \left[ \cos \varphi - \cos \theta_{Ch} \frac{n_{THz}}{n_r(\omega)} \right]$ ,  $D(\omega, \varphi) = \text{sinc}(K y_0 / 2)$ ,  $K(\omega, \varphi) = (k \sin \varphi - \Delta k \tan \theta_{Ch})$ .

Because  $L_x \gg y_0$  the THz-wave angular distribution is mainly determined by the factor  $F(\omega, \varphi)$  in (11) and, therefore, the direction of maximum emission at the central frequency  $\omega_{THz} = 2\pi/\lambda_{THz}$  is determined by  $\varphi = \theta_{Ch}$ . Under this condition the factor  $D(\omega_{THz}, \theta_{Ch}) = 2/\pi$  and in the following, to simplify calculations, we assume  $D(\omega, \theta_{Ch}) \approx 2/\pi$  for the entire spectrum of generated THz-waves. The resultant THz field is the sum of fields radiated by all beamlets and is given by

$$E_{THz}(\omega, \varphi) = \sum_{p=-N/2}^{N/2} E_{zp}(\omega, \varphi) \approx \frac{2Ae^{-ikR}}{\pi R} I_0 e^{-\frac{\omega^2 \tau_L^2}{4}} F(\omega, \varphi) \Phi(\omega, \varphi), \quad (12)$$

where  $\Phi(\omega, \varphi) = \sum_{p=-N/2}^{N/2} \exp \left\{ ip \left[ \frac{\omega}{c} n_r(\omega) y_0 \sin \varphi - \Delta k y_0 \tan \theta_{Ch} - x_0 (n_{gm} - 1) \right] \right\} \exp \left[ -2 \left( p y_0 / r_y \right)^2 \right]$ . (13)

From above it follows that at the central frequency  $\omega = \omega_{THz}$  and  $\varphi = \theta_{Ch}$  the factor  $\Phi(\omega_{THz}, \theta_{Ch}) = N + 1$ , if mask sizes  $y_0, x_0$  are satisfied by Eqs. (2), (3) and crystal is uniformly illuminated  $r_y \gg N y_0$ . Thus, the developed theoretical model confirms that the designed MSPM provides constructive overlapping of THz fields generated by every  $p$ -beamlet.

Fig. 2 shows the calculated THz field angular distribution for ZnTe (sLN) crystals at frequency  $\omega_{THz} = 2\pi$  THz by substituting in (12) and (13) the following values:  $d_{eff} = 68.5$  (168) pm/V [38],  $L_x = 10.4$  (3.5) mm [33, 31],  $y_0 = 98.0$  (33.7)  $\mu\text{m}$ ,  $I_{av} = 13.5$  (20) GW/cm<sup>2</sup>,  $n_0 = 2.73$  (2.15),  $N = 30$ ,  $x_0 = 200$   $\mu\text{m}$ ,  $\tau_L = 225$  fs,  $R = 30$  cm,  $r_z = 4$  mm. The pump beam waist radius is chosen to be  $r_y = Y_0/2 = 1.5$  (0.5) mm for ZnTe (sLN) crystals, respectively, that corresponds to intensity decrease of the at crystal edges by a factor of  $e^2$  compared to the on-axis value.

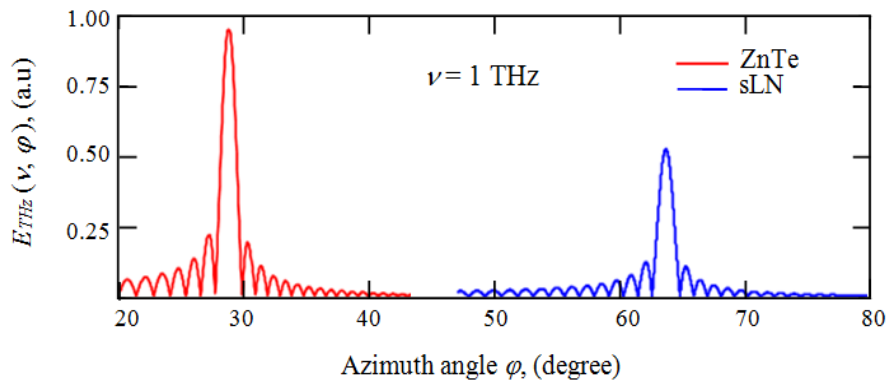


Figure 2. THz electric field strength in the frequency domain as a function of the radiation angle for ZnTe and sLN crystals at 1 THz frequency, respectively.

As was expected, it is seen from Fig. 2 that the THz field is mostly radiated in the direction of Cherenkov angles, which are  $\theta_{Ch} = 28.7^\circ$  ( $63.6^\circ$ ) for ZnTe (sLN) crystals, respectively. The field strength at the radiation maximum for ZnTe crystal is about 2 times higher than that of sLN crystal. The beams angular width at 3 dB level is approximately the same  $\Delta\varphi \approx 0.97^\circ$  for both crystals, which agree well with the predicted value from linear antenna theory [39]:

$$\Delta\varphi = \frac{0.886\lambda_{\text{THz}}}{n_{\text{THz}}L_x \sin\theta_{\text{Ch}}} \quad (14)$$

Using Parseval's theorem [40], the THz pulse energy spectral density is approximately given by

$$\varepsilon_{\text{THz}}(\nu) = \frac{n_{\text{THz}}}{2W} |E_{\text{THz}}(\nu, \theta_{\text{Ch}})|^2 R^2 \Delta\varphi \Delta\theta_z, \quad (15)$$

Here  $\nu = \omega/2\pi$  is the linear frequency and  $\Delta\theta_z$  is the beam width in meridional plane, which is estimated  $\Delta\theta_z \approx 1^\circ$  using Eq. (10) with  $r_z = 4$  mm. The calculation results for the energy spectral density  $\varepsilon_{\text{THz}}(\nu)$  as a function of the frequency for ZnTe and sLN crystals are presented in Fig. 3.

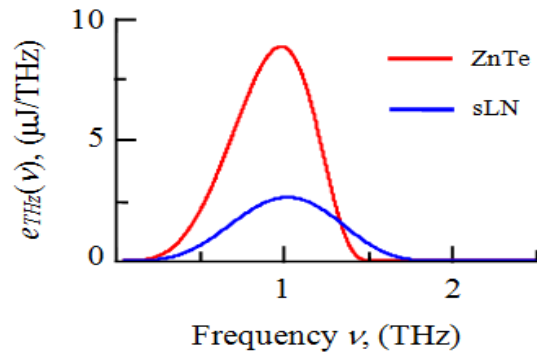


Figure 3. Dependencies of THz pulses energy densities on frequency for ZnTe and LN crystals.

From Fig. 3 it follows that for ZnTe crystal the spectral component at the central frequency  $\nu_0 = 1$  THz is about 3.4 times larger compared with that of LN crystal. It is mainly related to both significantly larger effective length  $L_e$  and largest possible dimension  $Y_0$  for ZnTe crystal. From Fig. 3 it is also seen that THz spectrum generated in ZnTe crystal is slightly asymmetric relative to the central frequency of 1 THz. This is attributed to strong THz dispersion in ZnTe crystal for frequencies above 1.7 THz.

By integrating the THz pulse energy spectral density  $\varepsilon_{\text{THz}}(\nu)$ , THz pulse energies are estimated as 10.5  $\mu\text{J}$  and 4.5  $\mu\text{J}$  for ZnTe and sLN crystals, respectively. As it was already mentioned, the highest average intensities were chosen  $I_{\text{av}} = 13.5$   $\text{GW}/\text{cm}^2$  (20  $\text{GW}/\text{cm}^2$ ), corresponding to the pump pulse energies 0.9 mJ (0.46 mJ) in ZnTe (sLN) crystals, respectively. Femtosecond pump sources with energies of 200 mJ and 90 mJ at wavelengths of 1.03  $\mu\text{m}$  and 1.7  $\mu\text{m}$  are available [41, 8]. Therefore, it is possible to increase significantly the above estimated THz pulse energies by applying higher pump energies. However, we do not present here numerical estimations, since the developed simple model makes it possible to obtain analytical expressions only at relatively low intensities where MPA and cascade processes do not become essential. This difficulty can be overcome by numerical calculations involving above mentioned and other nonlinear processes, which is a subject of our future work.

#### 4. CONCLUSIONS

In conclusion, it has been shown that the QPM generation of THz-pulses can be obtained by using a multistep phase mask contacting the entrance surface of a nonlinear crystal. The required dimensions of the mask steps were calculated for both ZnTe and LN crystals. The optimal number of steps in the mask was also estimated, taking into account individual beamlet's spatial broadening and problems related to the mask fabrication. Comparative analysis of THz-pulse generation by MSPM in ZnTe and LN crystals showed that application of ZnTe crystal is more preferable, especially when longer-wavelength laser is used as a pump source. The THz pulse energies are estimated as 10.5  $\mu\text{J}$  (4.5  $\mu\text{J}$ ) at relatively modest pump intensities 13.5  $\text{GW}/\text{cm}^2$  (20  $\text{GW}/\text{cm}^2$ ) for ZnTe (sLN) crystals, respectively. The proposed method is a promising way to develop high-energy, monolithic and alignment-free THz-pulse sources.

## ACKNOWLEDGMENTS

This work is supported by the Armenia MES State Committee of Science in the frames of the research project 15T-6B245. The help of Dr. H. Chosrowjan is acknowledged.

\*yuriav@ysu.am; phone 374 93544316; fax 37410- 554641; [www.yasu.am/faculties/en/Radiophysics](http://www.yasu.am/faculties/en/Radiophysics)

## REFERENCES

- [1] Hebling J., Yeh K.-L., Hoffmann M. C., and Nelson K. A., "High-Power THz Generation, THz Nonlinear Optics, and THz Nonlinear Spectroscopy," *IEEE J. Sel. Top. Quantum Electron.* 14, 345-353 (2008).
- [2] Hoffmann M. C and Fülöp J. A., "Intense ultrashort terahertz pulses: generation and applications," *J. Phys. D: Appl. Phys.* 44, 083001 (2011).
- [3] Kampfrath T., Tanaka K., and Nelson K. A., "Resonant and nonresonant control over matter and light by intense terahertz transients," *Nat. Photonics* 7, 680–690 (2013).
- [4] Hirori H., Nagai M., and Tanaka K., "Excitonic interactions with intense terahertz pulses in ZnSe/ZnMgSSe multiple quantum wells," *Phys. Rev. B.* 81, 081305 (2010).
- [5] Pálfalvi L., Fülöp J. A., Tóth Gy., and Hebling J., "Evanescent-wave proton postaccelerator driven by intense THz pulse," *Phys. Rev. ST Accel. Beams.* 17, 031301 (2014).
- [6] Nanni E. A., Huang W. R., Hong K.-H., Ravi K., Fallahi A., Moriena G., Miller R., and Kärtner F. X., "Terahertz-driven linear electron acceleration," *Nat. Commun.* 6, 8486 (2015).
- [7] Vicario C., Ovchinnikov A. V., Ashitkov S. I., Agranat M. B., Fortov V. E., and Hauri C. P., "Generation of 0.9-mJ THz pulses in DSTMS pumped by a Cr:Mg<sub>2</sub>SiO<sub>4</sub> laser," *Opt. Lett.* 39, 6632-6635 (2014).
- [8] Polónyi Gy., Monoszlai B., Gäumann G., Andriukaitis G., Balciunas T., Pugzlys A., Baltuska A., Feurer T., Hebling J., and Fülöp J. A., "High-energy terahertz pulses from semiconductors pumped beyond the three-photon absorption edge," *Opt. Express* 24, 23872-23882 (2016).
- [9] Ravi K., Huang W. R., Carbajo S., Wu X., and Kärtner F. X., "Limitations to THz generation by optical rectification using tilted pulse fronts," *Opt. Express* 22, 20239-20251 (2014).
- [10] Zhang C., Avestisyan Y., Abgaryan G., Kawayama, Murakami H., and Tonouchi M., "Tunable narrowband terahertz generation in lithium niobate crystals using a binary phase mask," *Opt. Lett.* 38, 953-955 (2013).
- [11] Hebling J., Almási G., Kozma I. Z., and Kuhl J., "Velocity matching by pulse front tilting for large-area THz-pulse generation," *Opt. Lett.* 10, 1161-1166 (2002).
- [12] Fülöp J. A., Ollmann Z., Lombosi C., Skrobel C., Klingebiel S., Pálfalvi L., Krausz F., Karsch S., and Hebling J., "Efficient generation of THz pulses with 0.4 mJ energy," *Opt. Express* 22, 20155-20163 (2014).
- [13] Huang S.-W., Granados E., Huang W. R., Hong K.-H., Zapata L. E., and Kärtner F. X., "High conversion efficiency, high energy terahertz pulses by optical rectification in cryogenically cooled lithium niobate," *Opt. Lett.* 38, 796-798 (2013).
- [14] Blanchard F., Ropagnol X., Hafez H., Razavipour H., Bolduc M., Morandotti R., Ozaki T., and Cooke D. G., "Effect of extreme pump pulse reshaping on intense terahertz emission in lithium niobate at multimillijoule pump energies," *Opt. Lett.* 39, 4333-4336 (2014).
- [15] Ofori-Okai B. K., Sivarajah P., Huang W. R., and Nelson K. A., "THz generation using a reflective stair-step echelon," *Opt. Express* 24, 5057-5068 (2016).
- [16] Zhong S., Li Ju., Zhai Z., Zhu L., Li Ji., Zhou P., Zhao J., and Li Ze., "Generation of 0.19-mJ THz pulses in LiNbO<sub>3</sub> driven by 800-nm femtosecond laser," *Opt. Express* 24, 14828-14835 (2016).
- [17] Ravi K., Ofori-Okai B. K., Sivarajah P., Huang W. R., Kärtner F. X., and Nelson K. A., "Broadband terahertz generation with a stair-step echelon," *CLEO OSA Technical Digest Series. STu3J.1* (2017).
- [18] Pálfalvi L., Fülöp J. A., Almási G., and Hebling J., "Novel setups for extremely high power single-cycle terahertz pulse generation by optical rectification," *Appl. Phys. Lett.* 92, 171107 (2008).
- [19] Yoshida F., Nagashima K., Tsubouchi M., Maruyama M., and Ochi Y., "THz pulse generation using a contact grating device composed of TiO<sub>2</sub>/SiO<sub>2</sub> thin films on LiNbO<sub>3</sub> crystal," *J. Appl. Phys.* 120, 183103 (2016).

- [20] Fülöp J. A., Polónyi G., Monoszlai B., Andriukaitis G., Balciunas T., Pugzlys A., Arthur G., Baltuska A., and Hebling J., “Highly efficient scalable monolithic semiconductor terahertz pulse source,” *Optica* 3, 1075-1078 (2016).
- [21] Abgaryan G., Makaryan A., Tadevosyan V., and Avetisyan Y., “Broadband THz generation in lithium niobate crystal by step-wise phase mask”, *Proc. of Microwave and THz Technique and Applications*, Gitutium NAS RA, pp. 13-16 (2015).
- [22] Avetisyan Y. and Tonouchi M., “Terahertz generation in QPM structure formed by a phase mask,” *Opt. Lett.* 37, 4155-4157 (2012).
- [23] L’huillier J., Torosyan G., Theuer M., Avetisyan Y., and Beigang R., “Generation of THz radiation using bulk, periodically and aperiodically poled lithium niobate - Part 1: Theory,” *Appl. Phys. B.* 86, 185-196 (2007).
- [24] Vodopyanov K. L., “Optical THz-wave generation with periodically-inverted GaAs,” *Laser and Photon. Rev.* 2, 11-25 (2008).
- [25] Fejer M. M., Magel G. A., Jundt D. H., and Byer R. L., “Quasi-phase-matched second harmonic generation: tuning and tolerances,” *IEEE J. Quantum Electron.* 28, 2631-2654 (1992).
- [26] Avetisyan Y., Zhang C., Kawayama I., Murakami H., Somekawa T., Chosrowjan H., Fujita M., and Tonouchi M., “Terahertz generation by optical rectification in lithium niobate crystal using a shadow mask,” *Opt. Express* 20, 25752-25757 (2012).
- [27] Jiang Y., Li D., Ding Y. J., and Zotova I. B., “Terahertz generation based on parametric conversion: from saturation of conversion efficiency to back conversion,” *Opt. Lett.* 36, 1608-1610 (2011).
- [28] Zheng D., Gordon L. A., Wu Y. S., Feigelson R. S., Fejer M. M., Byer R. L., and Vodopyanov K. L., “16- $\mu$ m infrared generation by difference frequency mixing in diffusion-bonded-stacked GaAs,” *Opt. Lett.* 23, 1010-1012 (1998).
- [29] Kubota T., Atarashi H., and Shoji I., “Fabrication of quasi-phase-matching stack of GaAs plates using a new technique: room-temperature bonding,” *Advanced Solid-State Photonics*, OSA Technical Digest Series, ATu5A.6 (2016).
- [30] Gayer O., Sacks Z., Galun E., and Arie A., “Temperature and wavelength dependent refractive index equations for MgO-doped congruent and stoichiometric LiNbO<sub>3</sub>,” *Appl. Phys. B.* 91, 343-348 (2008).
- [31] Palfalvi L., Hebling J., Kuhl J., Peter A., and Polgar K., “Temperature dependence of the absorption and refraction of Mg-doped congruent and stoichiometric LiNbO<sub>3</sub> in the THz range,” *J. Appl. Phys.* 97, 123505 (2005).
- [32] Marple D. T. F., “Refractive index of ZnSe, ZnTe, and CdTe,” *J. Appl. Phys.* 35, 539-541 (1964).
- [33] Tripathi S. R., Aoki M., Takeda M., Asahi T., Hosako I. and Hiromot N., “Accurate Complex Refractive Index with Standard Deviation of ZnTe Measured by Terahertz Time Domain Spectroscopy,” *Jap. J. Appl. Phys.* 52, 042401 (2013).
- [34] Fülöp J. A., Pálfalvi L., Almási G., and Hebling J., “Design of high-energy terahertz sources based on optical rectification,” *Opt. Express* 18, 12311-12327 (2010).
- [35] Hoffmann M. C., Yeh K.-L., Hebling J., and Nelson K. A., “Efficient terahertz generation by optical rectification at 1035 nm,” *Opt. Express* 15, 11706-11713 (2007).
- [36] Avetisyan Y., Zhang C., and Tonouchi M., “Analysis of linewidth tunable terahertz wave generation in periodically poled lithium niobate,” *J. Infrared Milli. Terahz Waves* 33, 989-998 (2012).
- [37] Schneider A., Neis M., Stillhart M., Ruiz B., Khan R., and Günter P., “Generation of terahertz pulses through optical rectification in organic DAST crystals: theory and experiment,” *J. Opt. Soc. Am. B* 23, 1822-1835 (2006).
- [38] Hebling J., Stepanov A. G., Almási G., Bartal B., and Kuhl J., “Tunable THz pulse generation by optical rectification of ultrashort laser pulses with tilted pulse fronts,” *Appl. Phys. B* 78, 593-599 (2004).
- [39] Stutzman V. L., Thiele G. A. [Antenna theory and design], Wiley, 239-244 (2013).
- [40] Saleh B. E., Teich M. C. [Fundamentals of Photonics], Wiley, 918-927 (1991).
- [41] Klingebiel S., Wandt C., Skrobol C., Ahmad I., Trushin S. A., Major Zs., Krausz F., and Karsch S., “High energy picosecond Yb:YAG CPA system at 10 Hz repetition rate for pumping optical parametric amplifiers,” *Opt. Express* 19, 5357-5363 (2011).